TKK Radio Science and Engineering Publications
Espoo 2009 REPORT R9

MODELS AND METHODS FOR COMPUTATIONAL ELECTROMAGNETIC DOSIMETRY

Thesis for the degree of Doctor of Science in Technology

Sami Ilvonen

Dissertation for the degree of Doctor of Science in Technology to be presented with due permission of the Faculty of Electronics, Communications, and Automation, for public examination and debate in Auditorium S4 at Helsinki University of Technology (Espoo, Finland) on the 10th of September, 2009, at 12 noon.

Helsinki University of Technology
Faculty of Electronics, Communications, and Automation
Department of Radio Science and Engineering

Distribution:
Helsinki University of Technology
Department of Radio Science and Engineering
P.O. Box 3000
FI-02015 TKK
Tel. +358 9 451 2261
Fax +358 9 451 2267
E-mail: ari.sihvola@tkk.fi

ISBN 978-952-248-008-8 (paper)
ISBN 978-952-248-009-5 (electronic)
ISSN 1797-4364 (paper)
ISSN 1797-8467 (electronic)

ABSTRACT OF DOCTORAL DISSERTATION	HELSINKI UNIVERSITY OF TECHNOLOGY P. O. BOX 1000, FI-02015 TKK http://www.tkk.fi

Author Sami Ilvonen

Name of the dissertation

Models and methods for computational electromagnetic dosimetry

Manuscript submitted 20.4.2009	Manuscript revised
Date of the defence 10.9.2009	
☐ Monograph	☒ Article dissertation (summary + original articles)

Faculty	Faculty of Electronics, Communications and Automation
Department	Department of Radio Science and Engineering
Field of research	Computational Electromagnetics
Opponent(s)	Prof. Luc Martens
Supervisor	Prof. Keijo Nikoskinen
Instructor	Prof. Keijo Nikoskinen

Abstract

The interaction between electromagnetic fields and the human body is a very complicated issue. In most cases it is not possible to measure accurately the electrical response of the human body to external sources. Because of this computational methods are used as an aid when determining the safety levels for human exposure to electromagnetic fields.

In this thesis the field distribution caused by various sources is determined in different parts of the human body using detailed and anatomically correct human body models and computational methods. Both the distribution of electric currents induced by low-frequency magnetic fields and the absorption of radio-frequency fields are studied. The accuracy and reliability of the models and methods used is verified by comparing the acquired results to known closed-form solutions and calibration measurements.

The obtained results can be utilised in the reliability analysis of computational methods used in electromagnetic dosimetry. Furthermore, some of the results are needed, for example, in the safety guidelines of medical personnel working close to magnetic resonance imaging scanners.

Keywords Computational dosimetry, low-frequency magnetic fields, specific absorption rate	
ISBN (printed) 978-952-248-008-8	ISSN (printed) 1797-4364
ISBN (pdf) 978-952-248-009-5	ISSN (pdf) 1797-8467
Language English	Number of pages 50+65
Publisher Helsinki University of Technology	
Print distribution	
☒ The dissertation can be read at http://lib.tkk.fi/Diss/2009/isbn9789522480095	

VÄITÖSKIRJAN TIIVISTELMÄ	TEKNILLINEN KORKEAKOULU PL 1000, 02015 TKK http://www.tkk.fi

Tekijä Sami Ilvonen

Väitöskirjan nimi

Sähkömagneettisten kenttien laskennallisen dosimetrian malleja ja menetelmiä

Käsikirjoituksen päivämäärä 20.4.2009	Korjatun käsikirjoituksen päivämäärä
Väitöstilaisuuden ajankohta 10.9.2009	
☐ Monografia	☒ Yhdistelmäväitöskirja (yhteenveto + erillisartikkelit)

Tiedekunta	Elektroniikan, tietoliikenteen ja automaation tiedekunta
Laitos	Radiotieteen ja -tekniikan laitos
Tutkimusala	Laskennallinen sähkömagnetiikka
Vastaväittäjä(t)	Prof. Luc Martens
Työn valvoja	Prof. Keijo Nikoskinen
Työn ohjaaja	Prof. Keijo Nikoskinen

Tiivistelmä

Ihmiskehon ja sähkömagneettisten kenttien välinen vuorovaikutus on hyvin monimutkainen ongelma. Useimmissa tapauksissa ulkopuolisten lähteiden ihmiskehon sisälle aiheuttamien kenttien voimakkuutta ei ole mahdollista määrittää tarkasti mittauksilla. Tämän vuoksi laskennallisia menetelmiä käytetään apuna määriteltäessä turvallisuusrajoja sähkömagneettisille kentille.

Tässä väitöskirjassa on tutkittu erityyppisten lähteiden aiheuttamien sähkömagneettisten kenttien jakaumaa ja suuruutta ihmiskehon eri osissa käyttäen laskennallisia menetelmiä sekä yksityiskohtaisia, anatomisesti tarkkoja kehomalleja. Työssä on tarkasteltu sekä matalataajuisten magneettikenttien indusoimien virtojen jakaumia että tehon absorboitumista radiotaajuisista kentistä. Käytettyjen menetelmien sekä lähdemallien luotettavuutta on tarkasteltu vertaamalla saatuja tuloksia tunnettuihin analyyttisiin tuloksiin ja kalibrointimittauksiin.

Väitöskirjan tuloksia voidaan hyödyntää arvioitaessa laskennallisten menetelmien luotettavuutta sähkömagneettisten kenttien dosimetriassa. Osaa saaduista tuloksista tarvitaan myös laadittaessa turvaohjeistusta esim. magneettikuvantamislaitteiden läheisyydessä työskentelevälle hoitohenkilökunnalle.

Asiasanat Laskennallinen dosimetria, matalataajuiset magneettikentät, ominaisabsorbtionopeus

ISBN (painettu) 978-952-248-008-8	ISSN (painettu) 1797-4364
ISBN (pdf) 978-952-248-009-5	ISSN (pdf) 1797-8467
Kieli Englanti	Sivumäärä 50+65

Julkaisija Teknillinen korkeakoulu

Painetun väitöskirjan jakelu

☒ Luettavissa verkossa osoitteessa http://lib.tkk.fi/Diss/2009/isbn9789522480095

Preface

This thesis work was carried out in the former Electromagnetics Laboratory and in the electromagnetics research group of the Department of Radio Science and Technology. The research work was financially supported by Graduate School in Electronics, Telecommunications and Automation and Graduate School of Applied Electromagnetics.

I wish to express my gratitude to my supervisors and colleagues. First of all, I am very thankful to Professor Keijo Nikoskinen for his guidance and efforts. The support and teaching I got from Academy Professors Sihvola and Lindell was also very helpful. I am also thankful for the lessons by Professor Sarvas. My sincere thanks to all co-authors, especially Ilkka Laakso and Tero Uusitupa. I thank the rest of the staff of the electromagnetics group, and particularly Jari and Henrik.

The support I got from the Radiation and Nuclear Safety Authority's personnel was very important for this work. The discussions about the practical issues in the dosimetry of electromagnetic fields and the measurement data were very valuable for my research. Thank you Kari, Lauri, Tommi, Tim, Sami and Ari-Pekka.

I also wish to thank William Martin from the Faculty of Electronics, Communication and Automation for consultation on the language and readability of the thesis.

Last but not least a warm hearted thanks for all my friends and relatives.

Espoo, April 2009

Sami Ilvonen

Contents

List of Publications

This thesis consists of an overview and the following publications which are referred to in the text by their Roman numerals.

I S. Ilvonen, A.-P. Sihvonen, K. Kärkkäinen, and J. Sarvas, "Numerical assessment of induced ELF currents in the human head due to the battery current of a digital mobile phone," *Bioelectromagnetics*, 26(8):648–656, Dec 2005.

II S. Ilvonen and J. Sarvas, "Magnetic-field-induced ELF currents in a human body by the use of a GSM phone," *IEEE Transactions on Electromagnetic Compatibility*, 49(2):294–301, May 2007.

III I. Laakso, S. Ilvonen, and T. Uusitupa. "Performance of convolutional PML absorbing boundary conditions in finite-difference time-domain SAR calculations," *Physics in Medicine and Biology*, 52(23):7183–7192, Dec 2007.

IV T. M. Uusitupa, S. A. Ilvonen, I. M. Laakso, and K. I. Nikoskinen. "The effect of finite-difference time-domain resolution and power-loss computation method on SAR values in plane-wave exposure of Zubal phantom," *Physics in Medicine and Biology*, 53(2):445–452, Jan 2008.

V S. Ilvonen, T. Toivonen, T. Toivo, T. Uusitupa, and I. Laakso. "Numerical specific absorption rate analysis and measurement of a small indoor base station antenna," *Microwave and Optical Technology Letters*, 50(10):2516–2521, Oct 2008.

VI S. Ilvonen and I. Laakso. "Computational estimation of magnetically induced electric fields in a rotating head," *Physics in Medicine and Biology*, 54(2):341–351, Jan 2009.

Author's Contribution

I The author was the principal writer of the manuscript and implemented the FEM solver program. The measurements, equivalent model implementation, FIT theory and solver were done by other authors. The other authors also participated in the preparation of the manuscript.

II The author was the principal writer of the manuscript, implementing the solver as well as computing and analysing the results. The least-squares fitting implementation for the determination of the dipole moments for the equivalent source was done by the second author.

III The author implemented the solver that was used to compute the results for large objects and participated in the study design.

IV The author implemented the parallel FDTD solver that was used in the study and contributed to the processing of the body models and simulation results.

V The author was the principal writer of the study and implemented all programming, modelling and data analysis in the publication. The other authors contributed the very valuable measurement results and processed the body model for simulation. The other authors also participated in the preparation of the measurement section of the manuscript.

VI This publication was the result of close co-operation between the authors. The author of this thesis was responsible for the research idea and implementation of the FEM solver. The second author was responsible for performing the post-processing work of the results. Both authors participated in the preparation of the manuscript.

List of Abbreviations

ABC	Absorbing Boundary Condition
CPML	Convolutional Perfectly Matched Layer
CNS	Central Nervous System
CSF	Cerebrospinal Fluid
CT	Computed Tomography
ELF	Extremely Low-Frequency
EM	Electromagnetic
FDTD	Finite-Difference Time-Domain
FEM	Finite-Element Method
FIT	Finite-Integration Technique
GSM	Global System for Mobile communications
ICNIRP	International Commission on Non-Ionizing Radiation Protection
MHD	Magnetohydrodynamic
MPE	Maximum Permissible Exposure
MRI	Magnetic Resonance Imaging
PDE	Partial Differential Equation
PML	Perfectly Matched Layer
PNS	Peripheral Nerve Stimulation
RF	Radio Frequency
RMS	Root Mean Square
SAR	Specific Absorption Rate
SPFD	Scalar-Potential Finite-Difference
WBA	Whole-Body Average

List of Figures

List of Tables

1 Introduction

The effect of electromagnetic fields on biological tissues has been known for a long time. Luigi Galvani and his experiments with prepared frog legs in the 18th century laid the basis for the systematic study of the subject [1]. As the knowledge grew and more powerful sources of electric current became available, it was evident that strong galvanic currents disturb the bioelectric processes in living organisms. At the end of the 19th century, when the incandescent light bulb was developed and widespread electrification began, safety concerns became a smear campaign in a corporate battle between Edison and Westinghouse over the direct versus alternating current for power transfer [2]. Alternating current became the standard adopted due to technical superiority and the fact that it is not considerably more dangerous than direct current. As a further consequence of this battle, electricity also left its marks on the history of capital punishment.

Electrification continued in the 20th century and as a result, electric power distribution is pervasive in modern industrialised societies. As technology progressed, new sources of electromagnetic fields came into public use. The utilisation of radio waves, especially personal wireless communication devices, has shaped the electromagnetic spectrum. Furthermore, knowledge about the interaction between electromagnetic fields and biological systems has grown. Understanding these mechanisms is essential in modern health care and many diagnostic tools, such as the *electroencephalogram (EEG)*, are directly based on the measurement and analysis of electromagnetic signals generated by the human body.

As strong fields can be detrimental to living organisms, the operation of electrical devices is controlled by laws and regulations. These regulations are based on the current scientific knowledge on the effects of the fields. Before appropriate safety levels can be determined, one has to know how the fields are distributed in and around the human body. In many cases, this can be a challenging problem by itself and often this information is approximated by using *worst-case* estimates. The purpose of this thesis is to study different cases where the human body is exposed to electromagnetic fields, estimating the distribution of resulting fields inside the human body using computational methods.

1.1 Scope of the Thesis

As this thesis consists solely of studies on how the electromagnetic fields are distributed inside the human body, it cannot answer the question how the given field distribution affects the biological system, and further, if the given fields have any effect in the short or long term. The interaction mechanisms between biological tissues and electromagnetic fields have been and are still being studied in many research groups all around the world. What this study does contribute is information on *how in certain cases the external field intensity is connected to field intensities inside humans*. Without this information the effects of external field intensities cannot be estimated accurately. A broader view on the field of this study can be found for example in [3].

2 Electromagnetics

2.1 Maxwell's Equations

Electromagnetic phenomena are governed by Maxwell's equations. Assuming time-harmonic fields with one constant angular frequency ω and complex harmonic time dependency $e^{j\omega t}$ with the imaginary unit j, Maxwell's equation can be written as

$$\begin{aligned} \nabla \times \mathbf{E}(\mathbf{r}) &= -j\omega\mathbf{B}(\mathbf{r}) && (2.1)\\ \nabla \times \mathbf{H}(\mathbf{r}) &= j\omega\mathbf{D}(\mathbf{r}) + \mathbf{J}(\mathbf{r}) && (2.2)\\ \nabla \cdot \mathbf{D}(\mathbf{r}) &= \varrho(\mathbf{r}) && (2.3)\\ \nabla \cdot \mathbf{B}(\mathbf{r}) &= 0 && (2.4) \end{aligned}$$

where $\varrho(\mathbf{r})$ is the source charge density, $\mathbf{E}(\mathbf{r})$ and $\mathbf{H}(\mathbf{r})$ are the electric and magnetic fields and $\mathbf{D}(\mathbf{r})$ and $\mathbf{B}(\mathbf{r})$ the electric and magnetic flux densities, respectively. The continuity equation of charge density and current density,

$$\nabla \cdot \mathbf{J}(\mathbf{r}) = -j\omega\varrho(\mathbf{r}), \tag{2.5}$$

is implicitly included in Equations 2.2 and 2.3. The electric and magnetic flux densities and corresponding fields are related by the constitutive relations

$$\begin{aligned} \mathbf{D}(\mathbf{r}) &= \varepsilon(\mathbf{r})\mathbf{E}(\mathbf{r}) && (2.6)\\ \mathbf{B}(\mathbf{r}) &= \mu(\mathbf{r})\mathbf{H}(\mathbf{r}), && (2.7) \end{aligned}$$

where $\varepsilon(\mathbf{r})$ is the electrical permittivity and $\mu(\mathbf{r})$ is the magnetic permeability, which is practically equal to that of the vacuum in biological tissues. In the presence of free charges, i.e. when the material has conductivity, we still need one equation. Considering a homogeneous bulk material, the electric field and current associated with the free charges are connected by the Ohm's law

$$\mathbf{J}(\mathbf{r}) = \sigma(\mathbf{r})\mathbf{E}(\mathbf{r}), \tag{2.8}$$

where $\sigma(\mathbf{r})$ is the conductivity of the material.

For different frequency ranges, biological tissues can be classified either as volume conductors or lossy dielectrics. The analysis of lossy dielectrics often uses the concept of complex permittivity. If the current term in Equation 2.2 is divided into ohmic and impressed parts, the ohmic and displacement current can be combined as

$$\nabla \times \mathbf{H}(\mathbf{r}) = j\omega\varepsilon_0 \underbrace{\left(\varepsilon_\mathrm{r}(\mathbf{r}) - \frac{j\sigma(\mathbf{r})}{\omega\varepsilon_0}\right)}_{\varepsilon_\mathrm{c}} \mathbf{E}(\mathbf{r}) + \mathbf{J}_\mathrm{i}(\mathbf{r}), \tag{2.9}$$

assuming that the material has isotropic relative permittivity of $\varepsilon(\mathbf{r})$ and conductivity of $\sigma(\mathbf{r})$. The ε_c is the complex permittivity, $\mathbf{J}_\mathrm{i}$ denotes the impressed source current and ε_r and ε_0 are the relative permittivity and permittivity of the vacuum, respectively.

2.1.1 Time-Domain Equations

In cases where the excitation is pulse or some other non-sinusoidal change, it is often advantageous to consider Maxwell's equations in the time domain. The time-domain equations can be constructed from Equations 2.1–2.2 by simply substituting $j\omega \rightarrow \partial_t$. In general cases the constitutive relations are more complicated. Assuming isotropic media with frequency dependency, the product in Equations 2.6 and 2.7 is transformed into a convolution. Evaluation of the convolution is a computationally expensive operation and this limits the applicability of time-domain techniques in such cases. However, if the material parameters can be assumed to be constant in the considered frequency range, the convolution is simplified to a simple product. The convolution due to some simple resonant material models can, however, be modelled using computationally efficient summation methods.

In the numerical dosimetry of electromagnetic fields, the most important implementation of the time-domain Maxwell's equations is the finite-difference time-domain (FDTD) method which is explained in more detail in Section 4.2. Another important case where the time-domain equations are very useful is the computation of fields induced by the movement in a static magnetic field. The static field does not induce any currents *per se*, but the movement of object even in a homogeneous static field causes the change of magnetic flux, i.e. $\partial_t \mathbf{B}(\mathbf{r}(t), t) \neq 0$. The movement in non-homogeneous magnetic fields has been studied *inter alia* in [4]. In the case of uniform rotation in a homogeneous magnetic field, such as in paper **VI**, the problem reduces back to a time-harmonic case.

2.2 Scalar-Potential Formulation for Low-Frequency Problems

Maxwell's equations can in many cases be solved more easily if the so-called *potentials* are used instead of the fundamental electromagnetic fields. As a thorough analysis of potentials can be found in several textbooks on electromagnetics, see for example [5], the details are omitted here. One example of a simpler solution procedure exploiting the potentials is the scalar potential finite-difference method (SPFD), which is a popular method for solving very low-frequency induction problems in computational electromagnetic dosimetry [6–8]. The advantage of SPFD compared to the other popular method, the impedance method [9], is the lower memory consumption due to scalar unknowns. Potential equations similar to the SPFD were used in papers **I**, **II** and **VI** with different exposure sources but the numerical solution process was, in fact, the finite-element method which is discussed in Section 4.3. Also, the modelling of sources is not straightforward and is discussed in Section 4.4.

If the frequency is very low, the wavelength in and outside the object under study becomes very large. This implies that the phase of the electric and magnetic fields can be assumed to have a constant value within and in the vicinity of the object thus allowing the use of *quasi-static approximation*. The term quasi is somewhat vague: in this context it should be understood so that some of the time derivatives of the fields are approximated to be zero while the time-dependent source term is not. In particular, when considering materials with conductivity, the first order induction term is present. On the other hand, from equation 2.9 we can see that the effect of the displacement current is negligible if $\varepsilon \ll \sigma/\omega$. As the validity of the quasi-static approximation depends not only on the frequency but also the dielectric properties of the object, it will be discussed in more detail in Section 3.1.

Let us shortly review how the scalar potential equation is formulated. If the permittivity

and conductivity are considered to be isotropic and piecewise homogeneous, and free space charges do not exist, Equations 2.1 and 2.5 can be written as

$$\nabla \times \mathbf{E}(\mathbf{r}) = -j\omega \mathbf{B}_0(\mathbf{r}) \tag{2.10}$$

$$\nabla \cdot (\sigma(\mathbf{r})\mathbf{E}(\mathbf{r})) = 0, \tag{2.11}$$

where $\mathbf{B}_0(\mathbf{r})$ denotes the external source magnetic flux density, which can be presented using a source vector potential $\mathbf{B}_0(\mathbf{r}) = \nabla \times \mathbf{A}_0(\mathbf{r})$. It is worth noticing that this vector potential is not unique. The same magnetic flux density can be presented using any vector potential of the form $\mathbf{A} \rightarrow \mathbf{A}_0 + \nabla\psi$, where ψ is a sufficiently smooth scalar function. This transformation is called *gauge transformation*, see [5] for more details. In practice the non-uniqueness of the source vector potential complicates the construction of the source term, as we will see in Section 4.4.1. Assuming that the $\mathbf{A}_0(\mathbf{r})$ is known, it can be substituted into Equation 2.10 and one gets

$$\nabla \times \underbrace{\left\{\mathbf{E}(\mathbf{r}) + j\omega \mathbf{A}_0(\mathbf{r})\right\}}_{-\nabla\phi(\mathbf{r})} = 0, \tag{2.12}$$

where the vector calculus identity $\nabla \times \nabla f \equiv 0$ has been used and ϕ denotes the unknown scalar potential. Combining this with Equation 2.11 gives a partial differential equation for the scalar potential $\phi(\mathbf{r})$ as

$$\nabla \cdot \big(\sigma(\mathbf{r})\nabla\phi(\mathbf{r})\big) = -j\omega \nabla \cdot \big(\sigma(\mathbf{r})\mathbf{A}_0(\mathbf{r})\big). \tag{2.13}$$

After solving Equation 2.13 the induced electric field is readily computed as

$$\mathbf{E}(\mathbf{r}) = -\nabla\phi(\mathbf{r}) - j\omega \mathbf{A}_0(\mathbf{r}) \tag{2.14}$$

and the induced current density can be computed from Ohm's law 2.8. The boundary condition for the induced current is naturally $\mathbf{n} \cdot \mathbf{J}(\mathbf{r}) = 0$, from which the boundary condition for the scalar potential equation can be constructed as

$$-\mathbf{n} \cdot \nabla\phi(\mathbf{r}) = j\omega \mathbf{n} \cdot \mathbf{A}_0(\mathbf{r}). \tag{2.15}$$

Here $\mathbf{n}$ denotes a unit vector normal to the boundary. The corresponding time-domain equation has been used in papers **I** and **II**.

In this form the scalar potential equation does not take into account the eddy currents, as the source magnetic flux density and the corresponding vector potential $\mathbf{A}_0$ are both fixed. If the conductivity of the object is low, this first order approximation is sufficient. As the static conductivity of biological tissues is rather low, the magnetic flux density due to the induced current is negligible compared to the source flux density $\mathbf{B}_0(\mathbf{r})$. If there is, for example, a metallic implant inside the body, the traditional SPFD cannot be used as the eddy currents of the implant are not solved correctly. An extended solution process for such cases has been proposed in [10, 11].

3 Electromagnetic Fields and Biological Tissues

3.1 Electrical Properties of Tissues

The main principles and features of the macroscopic dielectric properties of tissues are well known, see for example [12] or [13]. In this section a short summary is given since the electrical parameters are crucial for dosimetric studies. The most comprehensive collection of dielectric properties of biological tissues up-to-date is based on the extensive work by Gabriel et al [14–16].

Biological tissues are in general very dispersive and they have three main relaxation regions α, β and γ at low, medium and high frequencies, respectively. There are also other dispersions, including, for example, δ dispersion, but they are smaller. Each of these dispersion regions can in the simplest form be understood to be caused by a polarisation mechanism with a relaxation time τ and the Debye model for the complex relative permittivity of the form

$$\varepsilon(\omega) = \varepsilon_\infty + \frac{\varepsilon_\mathrm{s} - \varepsilon_\infty}{1 + j\omega\tau}. \tag{3.1}$$

In practice the polarisation effects in biological tissues are more complicated and the corresponding dispersion regions are broadened. This effect is usually modelled using the Cole-Cole dispersion model

$$\varepsilon(\omega) = \varepsilon_\infty + \sum_n \frac{\varepsilon_n - \varepsilon_\infty}{1 + (j\omega\tau_n)^{(1-\alpha_n)}} + \frac{\sigma_\mathrm{i}}{j\omega\varepsilon_0}. \tag{3.2}$$

Here σ_i denotes the static ionic conductivity and α is the measure of dispersion broadening. As an example, the permittivity and conductivity of muscle tissue are shown in Figure 3.1. The parameters are those from [16].

As one can see, the relative permittivity of biological tissue can be extremely high compared to the materials common in technical applications. As the low-frequency solution methods presented in previous sections omitted the effect of the displacement current based on partially on the assumption that $\varepsilon \ll \sigma/\omega$, it seems that in some tissues at low frequencies the validity of this assumption should be questioned. This problem has been studied in [17], where the final conclusion was that the error due to the omitted displacement current in typical exposure calculations is small compared to the uncertainties of the material parameters.

3.2 Coupling Between Electromagnetic Fields and the Human Body

There are three currently established basic coupling mechanisms between the time varying electromagnetic fields and living matter [18]:

1. coupling through low-frequency electric field
2. coupling through low-frequency magnetic field
3. absorption of energy from electromagnetic fields

In this context the contact currents that are due to a physical contact between a biological body and a conducting object in a different potential are not considered to be a coupling mechanism between the fields and the material. The contact currents are, however, a

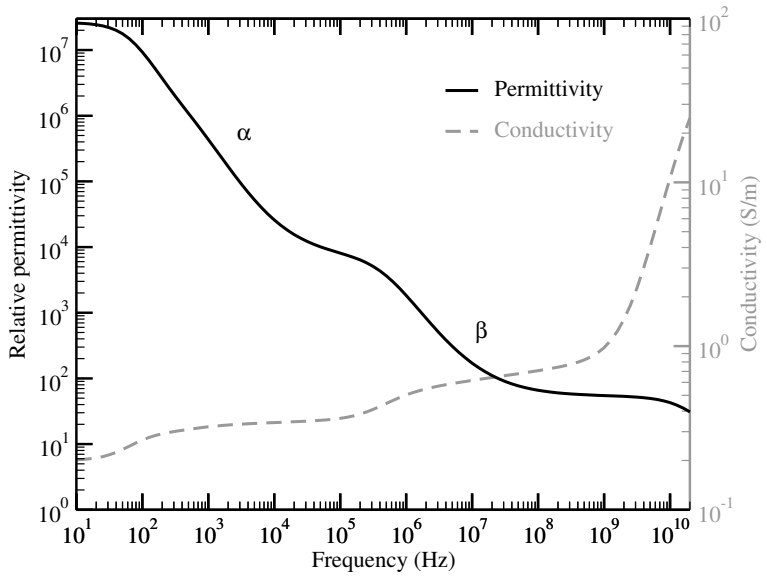

Figure 3.1: Permittivity and conductivity of muscle tissue according to [16]. The γ dispersion is present at higher frequencies.

very important for electrical safety. Neither the contact currents nor the coupling between low-frequency electric fields are studied in this thesis. Let us shortly summarise the main concept of coupling mechanisms 2 and 3, which are illustrated in Figure 3.2.

Low-frequency magnetic fields:

As the biological material is non-magnetic, as stated in Section 3.1, a static magnetic field penetrates a stationary body unperturbed. In the low-frequency region the changing magnetic field or movement of the body in the magnetic field induces electromotoric force and currents into a conducting media as explained in Section 2.2. These induction currents are solenoidal, i.e. $\nabla \cdot J = 0$. The changing magnetic field is usually due to a time-varying current.

Absorption of energy from electromagnetic fields:

At frequencies above about 100 kHz, significant absorption of energy is possible and can lead to a harmful temperature increase. The locations of absorption vary depending on the frequency and naturally on the source of exposure. At very high frequencies (tens of GHz) the power absorption is concentrated on the skin as the fields do not penetrate deeper into the body. In a frequency range from approximately 300 MHz to several GHz, significant local and nonuniform absorption can occur [18].

In both cases, nonuniform exposure is most difficult to assess as it cannot be described simply using a strength of field as a measure. The localised values depend on the exact geometry and operation of the source, hence each exposure case (source or device type) has to be considered separately.

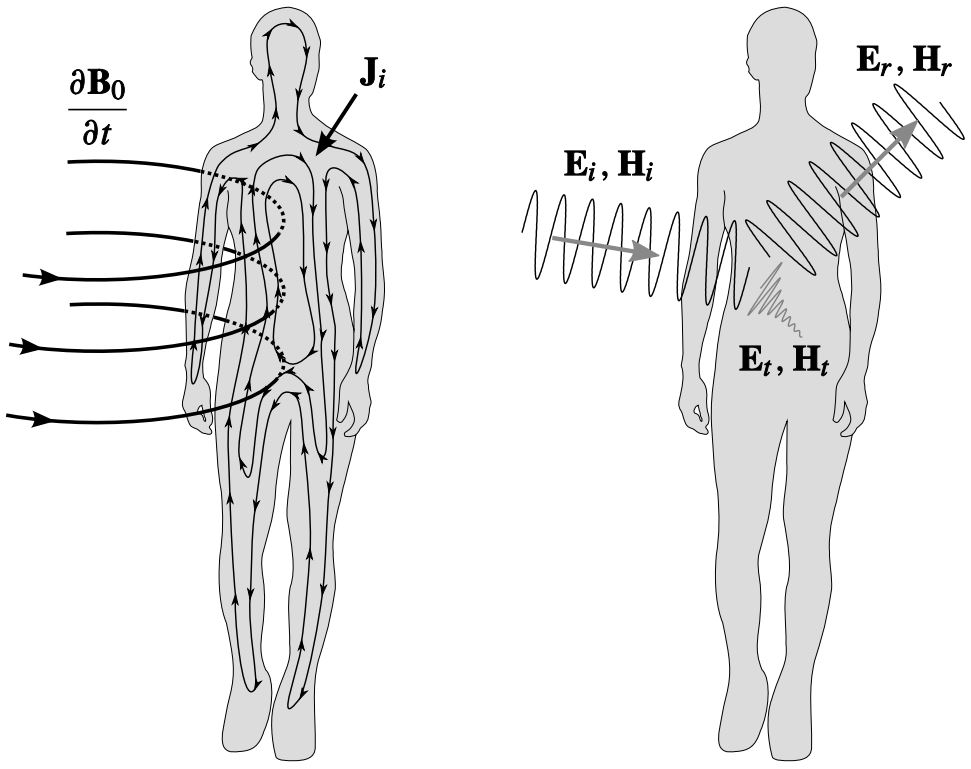

(a) Induction due to a changing external magnetic flux density.

(b) Absorption of power from a RF electromagnetic field.

Figure 3.2: The two electromagnetic coupling mechanisms studied in this thesis. In both cases the connection between the external sources and internal field intensities has a very complicated relation that can in practice be determined only numerically.

One important coupling mechanism between static fields and the human body is the induction of currents due to movement in static magnetic fields. The magnitude of the induced electric field due to head movements in a strong magnetic field has been measured in [19]. This type of coupling can cause significant physiological responses in the case of, for instance, MRI scanners.

3.3 Biological Basis for Restricting the Exposure

The biological effects of electromagnetic fields is a much studied, albeit not thoroughly mastered subject. Because the exposure to very strong electromagnetic fields has harmful effects, there is a need for protective regulation and even legislation. The regulations are based on known and well-established biological effects. The effects of these electromagnetic fields include, but are not limited to, the following [13]:

Peripheral nerve stimulation (PNS)

Peripheral nerves have an *all-or-nothing* response that can be triggered by an electric field, or equivalently by the ohmic current, that causes membrane depolarisation. The excitation threshold for membrane depolarisation is frequency dependent. In most severe cases, such as electric shocks, the PNS can affect the heart and cause cardiac arrhythmia.

Phosphenes

Phosphenes are a visual effect that is produced when the head is exposed to, for example, ELF electric currents or magnetic fields. They are caused by the modification of synaptic potentials in the retina due to the exposure. Phosphenes are perceived as light flashes and there are no known adverse effects associated with them. The threshold value of phosphenes is also frequency dependent with a minimum level at about 20 Hz.

Heating

The absorption of power from electromagnetic fields causes temperature rise in tissues. This is a very well established effect. The high levels of absorbed power can cause irreversible tissue damage. Eyes are particularly sensitive because the heat can cause cataracts [20].

Magnetohydrodynamic effect (MHD)

Magnetohydrodynamic effects are caused by the Lorentz force exerted to a charged particle, such as the ions in blood, moving in a magnetic field. These effects are often associated with very strong (in the order of 1 T or more) magnetic fields found in, for example, MRI scanners.

Vertigo

Strong magnetic fields can cause vertigo-like sensation and/or a feeling of movement. These effects are probably caused by the induced electric field that stimulates the hair cells in vestibular organ and the nerve cells connected to the vestibular system. The role of MHD effects has been questioned in a recent study [21] and the

magnetic susceptibility differences between the vestibular organs and the surrounding fluid together with the induction currents are proposed to be the reason behind the effects.

Auditory effects
Strong, pulsed microwave pulses can cause audible effects. It is assumed that these effects are due to very rapid thermoelastic expansion. As the required power levels are very high and the duration of the exposure has to be short, this effect is associated mostly with radars. A short summary of the effect is given in [22].

Electroporation
Strong electric fields cause pores in cellular membranes. If the field is strong enough, the damage is irreversible. The field intensity required for poration is rather high, making electroporation damages associated with accidents involving high-voltage contact currents. Electroporation is also used as tool in cellular biology as it provides a method to insert genes and chemicals into the interior of a cell.

Two most important effects with solid scientific background are the PNS and heating. These two effects have formed the basis for limiting the exposure to electromagnetic fields. The limits are discussed in more detail in Section 3.5.

In spite of continuous research, the long-term effects of low-level EMF exposure remain unclear. There are inconclusive results that suggest a connection between childhood leukaemia and ELF magnetic fields, see [23] for a summary of research on this topic. In addition to the mentioned effects, there are several proposed mechanisms on how the fields can interact with living tissue. The term proposed in this context means that effects may have a physical background but their reaction threshold in living human organism have not been or cannot be verified.

3.4 Limited Quantities

As both mechanism of coupling and the biological effect varies with frequency, different physical quantities have to be controlled to assure that no harmful effects due to exposure will occur. In the lower frequency range, the induced current or electric field is associated with the biological effects. In recent studies the electric field is determined to be more a reliable quantity, see for example [24] for a discussion on this topic. In higher frequency ranges, the generally accepted electrical parameter to be restricted is the *specific absorption rate* (SAR), which is defined as

$$\mathrm{SAR} = \frac{d}{dt}\left(\frac{dW}{dm}\right) = \frac{\sigma E_{\mathrm{rms}}^2}{\rho}, \tag{3.3}$$

where W (J) is the absorbed energy, m (kg) is the mass, ρ (kg m^{-3}) is the density and σ (S m^{-1}) the conductivity of the material. As the electric field can be measured inside, for example, a phantom, one can determine the SAR once the density and conductivity of the material (in practice tissue equivalent liquid) is known. The connection between the SAR and temperature can be established using the heat equation

$$\frac{dQ}{dT} = \rho V C, \tag{3.4}$$

where Q (J) is the thermal energy, T (K) is the temperature, V (m^3) is the volume and C (J kg^{-1} K^{-1}) the heat capacity. If we consider a small volume inside the body and assume an adiabatic system, i.e. the heat does not conduct or radiate from our selected volume, we get a worst case estimate to the heat rise during a period of Δt as

$$\Delta T = \frac{\Delta t}{C}\text{SAR}. \tag{3.5}$$

This estimate implies that the heat rises indefinitely as the exposure is non-zero. In practice, the heat conducts to adjacent regions which lowers the temperature when the exposure is localised. Moreover, respiration and evaporation processes and heat conduction to the surrounding air will cool the body. However, as a worst-case estimate the SAR values are useful. In practice the SAR values are evaluated as an average over a given mass. In the case of *whole-body average SAR* the averaging is done over the whole body. *Local average SAR* values are usually computed as an average over 1 g or 10 g mass.

As the SAR is associated with a unit mass, it is not a good quantity for frequencies above about 6 GHz, because the electromagnetic fields penetrate only to a very thin layer in the surface of the body. A more logical choice is to use a quantity that is proportional to the area instead of the volume or mass. In the exposure standards the limiting quantity for very high frequencies is power density. The power density is associated with a plane-wave solution of Maxwell's equations, which can be written as

$$\mathbf{E}(\mathbf{r}) = \mathbf{E}_0\, e^{-j\mathbf{k}\cdot\mathbf{r}}, \tag{3.6}$$

where $\mathbf{k}$ is the wave vector of the plane wave. Using this expression together with Equations 2.2 and 2.6 one can derive the corresponding expression for the magnetic field. From the electric and magnetic fields one can write the expression for the time-average power density of the plane wave as [5]

$$\mathbf{S}(\mathbf{r}) = \mathcal{R}\left\{\frac{1}{2}\mathbf{E}(\mathbf{r}) \times \mathbf{H}(\mathbf{r})^*\right\}, \tag{3.7}$$

where * denotes complex conjugation and both field values are assumed to be peak values. If the media where the plane wave propagates is a vacuum or air, the expression for power density can be simplified to

$$S = \frac{|\mathbf{E}|^2}{2\eta_0} = \frac{\eta_0|\mathbf{H}|^2}{2}, \tag{3.8}$$

where $\eta_0 \approx 377\ \Omega$ is the wave impedance of the vacuum.

3.5 Limits of Exposure to Electromagnetic Fields

To ensure the safety of humans, several national and international bodies have set protective standards and guidelines to limit the exposure to electromagnetic fields. Some of these standards are considered advisory, but often also the legislation is based on the guidelines and standards. In this section, only some guidances from two of bodies are presented. The first of these bodies is the IEEE (originally an acronym for the Institute of Electrical and Electronics Engineers) and the other is the International Commission on Non-Ionizing Radiation

Protection (ICNIRP). The following information is collected from IEEE standards [25, 26] and ICNIRP guidelines [18, 27]. As the knowledge of health effects grows, the standards and guidelines are updated and it should be noted that the two aforementioned IEEE standards are more recent than the ICNIRP guidelines. ICNIRP has also recently published new guidelines on limiting the exposure to static magnetic fields [28].

One common basic feature of these standards and guidelines is the concept of *basic restriction*. It is an *in situ* limit set for the physical quantity responsible for the adverse effect. As *in situ* values are very difficult to assess in complex environments, there are also *maximum permissible exposure* (MPE) limits used by IEEE and, similarly, *a reference level* used by ICNIRP that limits the exposure to the fields outside the body. For example, in the exposure scenario of Figure 3.2(a) the basic restriction is for the induced current (ICNIRP) or the *in vivo* electric field (IEEE) and the reference level for the source magnetic flux density $\mathbf{B}_0$. Of these two set of limits, the basic restriction is the one that should not be exceeded under any circumstances. These reference limits are set so that if the exposure is compliant with the reference level, the basic restriction cannot be exceeded. Ensuring that the reference levels are set correctly is one important application of numerical exposure calculations. The actual value for basic restriction is selected to be lower that the known threshold value for the adverse effect multiplied by a reasonable safety factor.

Another common feature in these exposure standards is the division into exposure of the general public and work-related (IEEE equivalent: controlled environment) exposure. The rationale behind this division is that the age and health status of the general public may be different from workers, and in controlled environments people can also be instructed and trained to avoid actions that increase the possible risks.

The basic restrictions recommended by ICNIRP are given in Table 3.1. The IEEE limits for the corresponding exposure scenarios is split between the two standards. The values for exposure to fields in the frequency range 0–3 kHz are given in Table 3.2. In a more recent standard [26], the applicability of these values is extended to frequencies below 5 MHz. The IEEE SAR basic restrictions for frequencies from 0.1 to 3 MHz are shown in Table 3.3. In the range 0.1–5 MHz both the *in situ* electric field and the SAR have a basic restriction. In the ICNIRP guideline, the same overlap is present for the induced current density and the SAR values in the range from 0.1 to 10 MHz.

Comparing Tables 3.1 and 3.3 shows that the SAR basic restrictions for the exposure are equal except for the technical details on application. At the lower end of the frequency spectrum, the comparison of the limits is more complicated as different physical quantities are used. The ICNIRP guideline [18] limits the induced currents density while the electric field is used by the IEEE in [25]. These two quantities are linked by the conductivity, which depends on the tissue and the frequency. As the uncertainties in conductivities in that particular frequency range is rather large and the values are also frequency dependent, the comparison is not straightforward. In addition, the IEEE limits are given separately to different parts of the body including the heart.

In the recent ICNIRP guideline [28] the limit for general public exposure to static magnetic field is 400 mT. For occupational exposure the limit is 2 T for head and trunk and 8 T for the limbs.

3.5.1 Computational Considerations

The biological responses mentioned in Section 3.3 differ from each other considerably. Some effects, such as the phosphenes and PNS, are very localised, while others, such as heating, are general to the whole body. It is also known that the resolution of numerical simulations affects the results which is also something noted in papers **II** and **IV**. Averaging diminishes these differences and makes the computational results less dependent on small geometrical and resolution differences. In addition, there are also physiological reasons for the averaging. For nerves, for example, the excitation threshold depends on both the temporal and spatial gradient of the electric field and therefore averaging of the external electric field over a distance of 5 mm has been suggested [29].

As a result, the basic restrictions presented in Section 3.5 are given for locally averaged values, except for the whole-body averaged SAR. Depending on the problem in hand and the method of simulation, these averaging processes can lead to problems, as noted in [30]. In general, the standards often do not give very detailed instruction on the process of averaging. For example, the shape of the averaging volume of the localised SAR values is not fixed in the ICNIRP guidelines. Especially at the higher end of the frequency spectrum, the shape of the averaging volume can have a strong influence on the values, since the SAR decreases rapidly inside the tissues. Finding the maximum value from all possible shapes of 10 g volumes is not computationally feasible and, in practice, one usually selects a simple volume such as a cube. These ambiguities make the comparison of published results challenging.

On the other hand, very detailed descriptions of the modelling process and averaging can rule out some numerical methods. For example, the averaging process presented in [31] is not easily adaptable to tetrahedral meshes that are commonly used in finite-element modelling.

Table 3.1: ICNIRP basic restrictions as given in [18]. Here f denotes the frequency in hertz. Exact conditions for applying the limits, including the averaging, are given in the original guideline and are not repeated here.

Exposure characteristics	Frequency range	Current density for head and trunk (mA m^{-2}) (rms)	Whole-body average SAR (W kg^{-1})	Localised SAR (head and trunk) (W kg^{-1})	Localised SAR (limbs) (W kg^{-1})
Occupational exposure	up to 1 Hz	40	—	—	—
	1–4 Hz	40/f	—	—	—
	4 Hz–1 kHz	10	—	—	—
	1–100 kHz	f/100	—	—	—
	100 kHz–10 MHz	f/100	0.4	10	20
	10 MHz–10 GHz	—	0.4	10	20
General public exposure	up to 1 Hz	8	—	—	—
	1–4 Hz	8/f	—	—	—
	4 Hz–1 kHz	2	—	—	—
	1–100 kHz	f/500	—	—	—
	100 kHz–10 MHz	f/500	0.08	2	4
	10 MHz–10 GHz	—	0.08	2	4

Table 3.2: Basic restrictions from IEEE standard C95.6-2002 [25] for human exposure to electromagnetic fields at frequency range 0–3 kHz. E_0 is the minimum (rheobase) electric field. The *in situ* electric field is $E_\mathrm{i} = E_0$ for $f \leq f_\mathrm{e}$ and $E_\mathrm{i} = E_0(f/f_\mathrm{e})$ for $f \geq f_\mathrm{e}$. In addition to the listed restrictions, the standard limits the exposure of the head and torso to magnetic fields below 10 Hz to peak values of 167 mT for general public and 500 mT in the controlled environment. The frequency range of these limits is extended to 5 MHz in IEEE standard C95.1 [26].

Exposed tissue	f_e (Hz)	General public	Controlled environment
		E_0 rms (V m^{-1})	E_0 rms (V m^{-1})
Brain	20	5.89×10^{-3}	1.77×10^{-2}
Heart	167	0.943	0.943
Hands, wrists, feet, ankles	3350	2.10	2.10
Other tissue	3350	0.701	2.10

Table 3.3: Basic restrictions from IEEE standard C95.1-2005 [26] for human exposure to electromagnetic fields at frequency range 100 kHz–3 GHz. Here the action level is equivalent to the general public exposure level in Tables 3.1 and 3.2. Exact conditions for applying the limits, including the averaging, are given in the original standard and are not repeated here.

Exposure type	Averaging	Action level	Controlled environment
		SAR (W kg^{-1})	SAR (W kg^{-1})
Whole-body	WBA	0.08	0.4
Localised	10 g average	2	10
Extremities and pinnae	10 g average	4	20

4 Numerical Modelling

In the previous sections the electromagnetic and physiological background of dosimetric problems was presented. As the closed-form solutions for Maxwell's equations for arbitrary geometries and sources are not known, one has to use numerical methods or approximate the geometries. The first estimates of internal field distribution in humans were obtained using simplified models consisting of layered spheres and prolate ellipsoids [32,33]. An old summary of analytical techniques in electromagnetic field dosimetry can be found in [34]. It should be pointed out that many analytical solutions for simplified geometries are often also approximative even for the given simple geometry. One such example of a recent analytical solution for a layered lossy ellipsoid for bioelectromagnetic applications is given in [35]. Because the error resulting from the simplified geometry is impossible to control, numerical methods are essential for dosimetry involving realistic human body models. Analytical models, despite of their shortcomings, are useful for many other applications in dosimetry. In this section a short review of the numerical methods and models used in this thesis by the author is given.

4.1 Human Body Models

Accurate anatomical models are essential for dosimetric simulations. The first approximations of the internal field intensity were obtained using analytical models of simple ellipsoids and cylinders. As humans and animals are electrically very inhomogeneous and structurally very complicated, simple geometrical models do not give representative results on the field distribution inside the body. As there is a large variation in absolute and relative dimensions of humans, results obtained using a single model can not be used to derive general results. Therefore, a variety of models is needed for dosimetric purposes.

The advent of modern tomographic methods has made the construction of very detailed correct body models practical for many different purposes. For example, detailed computed tomography (CT) scans have been used as an additional tool to determine the cause of death [36]. If the model is constructed using a healthy volunteer, currently the MRI is the only practical method due to the low health risks involved. A whole body CT scan, for example, gives the subject a considerable dose of ionizing radiation.

The main problem in the model construction is that the data obtained from imaging methods cannot be directly mapped to electrical properties. Because of this, one has to identify the geometry of different internal structures and organs using the imaging data. As a result, one obtains a model with non-overlapping regions that present different tissues. In practice, current human models usually contain about fifty different tissues / organs. Good quality tissue segmentation is a time-consuming process and requires a good knowledge of the human anatomy. Several automated processes for the tissue segmentation has been proposed but usually only for a certain parts of the body as noise and other problems in the imaging often prevent fully automated processing, see e.g. [37] for a short review on the automatic tissue segmentation of the human brain. To overcome the shortcomings of imaging methods some projects have used several of them, as in the Visible Human Project [38] and a visible Korean human project [39].

The tissue segmentation is usually done layer by layer for each of the two-dimensional

Figure 4.1: Coronal slice from an anatomical model that consists of different, segregated tissues. Presented data is from Virtual Family project [40].

images and the three-dimensional model is then constructed from the individual images. As there are very complicated tissue boundaries, one usually has to carefully inspect that the different layers present the correct geometry and change the segmentation on adjacent layers. The result of this process is a rectangular parallelogram composed of small voxels (volume pixels) each presenting one of the segmented tissues. The resolution of the two-dimensional images and the distance between them determines the level of anatomical detail in the model. As resampling and even simple rotations cause interpolation errors, in some models the tissue boundaries are described as parametric curves instead of raster images. This data is then used to produce voxel or, for instance, tetrahedral models for a simulation. Even though the parametric presentation is "exact" in some sense, it is still limited by the accuracy of the original imaging data.

The aforementioned procedure generates a body model in a rigid, non-modifiable posture. This restriction is also partially due to the imaging methods, which cannot be used for the whole body in an arbitrary posture. However, often sitting or other postures are needed for the exposure assessment. The usual approach for posture variation is to modify a segmented voxel model. Naturally the stiffness of the tissues has to be taken into account in the process so that the shape of the bones does not change as they are rigid and the joints work correctly. The soft tissues are more complicated as their shape is dependent on the elasticity of the tissue and surrounding structures. An early example of modifying a standing voxel model can be found in [41]. A more detailed description on the process of constructing posturable Japanese male and female models is given in [42]. There are also commercial posturable models available, but they are often tied to a specific software environment. In this thesis all results have been computed using non-posturable models due to the poor availability of posturable models. The statistics of the whole-body human voxel models used in this thesis is given in Table 4.1. The table does not, however, include the head-only model used in paper **I**. The resolution of that model is $1.3\times1.3\times2.0$ mm and it consists of 15 different tissues though only the central nervous system (CNS) and cerebrospinal fluid (CSF) were used in the simulation.

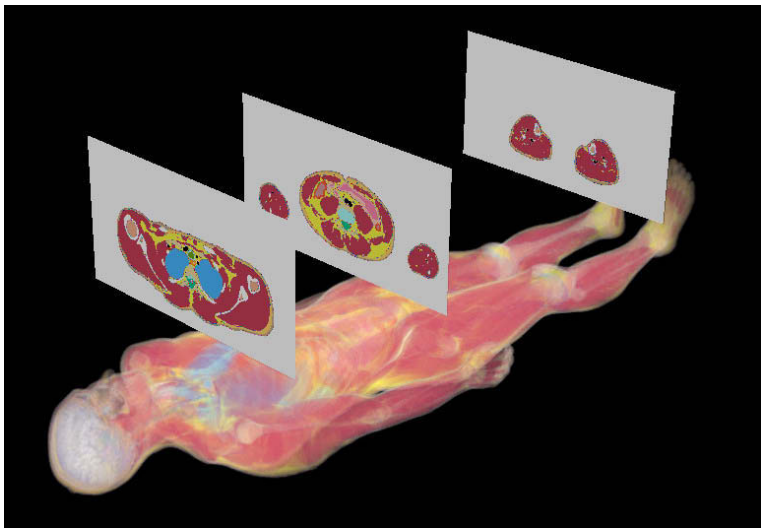

Figure 4.2: Volume rendering of a whole body model with three coronal slices. Data is from the Virtual Family model [40].

Table 4.1: List of human body models used in this thesis. The column *tissues* lists the number of segregated tissue types or anatomical parts.

Body model	Tissues	Resolution	Voxels
		(mm)	$\times 10^6$
BAFB	38	1.0	103
Norman	37	2.0	8.27
Hanako	51	2.0	6.28
Taro	51	2.0	7.98
Duke[†]	76	n/a	n/a
Ella[†]	76	n/a	n/a
Zubal	86	3.6	1.63

[†] Both Duke and Ella are models that have been converted to CAD format. In paper **VI** 1 mm and 2 mm resolution voxel models generated from these datasets have been used.

4.2 Finite-Difference Time-Domain Method

The finite-difference time-domain method [43] is a very popular numerical solution technique for electrodynamic problems. In fact one of the first important application of the FDTD method was determining the heating of the human eyes due to an RF exposure [44]. As there are many good textbooks that describe the FDTD method in great detail, for example [45], only a short summary is given here. It is good to notice that the FDTD is most suitable for high-frequency simulations where the object under study is on the scale of wave length or larger, though it has been used on the quasi-static frequency range. There are several commercial providers of electromagnetic field simulation software packages that utilise the FDTD method. In this thesis, however, all FDTD results were computed using a self-programmed solver.

In finite-difference methods the differential operators of the original PDE are approximated using *differences* and the solution is approximated in a set of points called a grid. When the curl operators in the time-domain versions of Equations 2.1 and 2.2 are approximated using central differences, one can after some manipulation construct the update equations for electric and magnetic field values distributed in a cartesian grid in space. One block of this grid is often called *Yee's cell*. The resulting FDTD grid can be presented as two overlapping grids, one for electric and another for magnetic field values. The spatial distribution of field values in these grids is shown in Figure 4.3, where one block of both grids is shown.

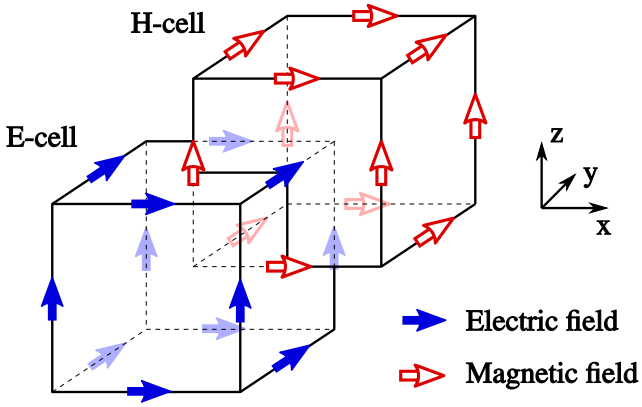

Figure 4.3: Location of electric and magnetic field components in the FDTD grid.

The FDTD method has many advantages compared to other high-frequency solving techniques for Maxwell's equations available for bioelectromagnetic problems. Due to the locality of the differences in the FDTD method, it is relatively easy to program a scalable and efficient parallel implementation of the method using simple spatial decomposition. This enables the simulation of very detailed models using parallel computers. Additionally, the modelling of very inhomogeneous and complex materials is relatively easy, although modelling complex structures made of conductive materials is one of the weaknesses of the FDTD method. As most of the body models consist of voxels, the inflexibility of the

cartesian grid is not a problem. There is also a plethora of scientific publications with different approaches for modelling complicated geometrical structures with variable levels of detail using the FDTD method.

Since the computational domain cannot be extended to infinity, an absorbing boundary condition is needed when simulating structures with an open boundary. This includes practically all the SAR simulations. Fortunately, the PML boundary conditions work efficiently in FDTD simulations. In [46] and in publication **III** the error due to the PML boundary condition in the SAR simulations was studied and the results show that the error due to PML can be made negligible. It should be noted though, that the application of PML boundaries is somewhat involved because there are several parameters that need to be selected correctly according to the properties of the simulation.

4.3 Finite Element Method

The finite-element method (FEM) is a very popular numerical method for solving partial differential equations. As it is widely used in many areas of engineering and science, there is a great many publications and textbooks available. One popular textbook on solving electromagnetic problems using the FEM is [47]. As the FEM is used only for quasi-static problems in this thesis, the problems associated with higher frequency problems are not discussed here. It is just acknowledged that the FEM has been used together with the boundary element method in [48, 49] and this procedure has its advantages as well as disadvantages when compared to the more traditional FDTD approach used in this thesis.

In the FEM, in contrast to the previously mentioned finite-difference methods, the solution of the PDE is approximated in a mesh that consists of elements with a finite domain (hence the name finite-element method). When modelling geometries in three-dimensional space, the usual choice for element is a tetrahedron because of its flexibility to model volumes with curved boundaries and different sized details as well as the relative ease of mesh generation for many engineering purposes. For detailed models of the human body having tens of different regions with complicated shapes, the mesh generation process becomes a very demanding task.

The first step in the FEM solution process is to reformulate the original differential operator form of the problem to a *weak form*, i.e. a relaxed form of the problem. The weak form satisfies the original problem on the average over the domain. This reformulation can be done using either by utilising the stationarity of a variational form, if one exists for the problem at hand, or by using a weighted residual procedure. If we take Equation 2.13 as an example, the weak form can be constructed using the weighted residual procedure by first multiplying the equation with a continuous test function and integrating over the domain as

$$\int_V v\nabla\cdot\sigma\nabla\phi\,dV = -j\omega\int_V v\nabla\cdot\sigma\mathbf{A}_0\,dV, \tag{4.1}$$

where v is the test function. The second step is to integrate the both sides by parts and apply and boundary condition 2.15. The result can be written as

$$\int_V \nabla v\cdot\sigma\nabla\phi\,dV = -j\omega\int_V \nabla v\cdot\sigma\mathbf{A}_0\,dV. \tag{4.2}$$

Now the original problem has been transformed to a form where we seek a function ϕ that fulfils Equation 4.2 for *every* v. It can be shown that solution of Equation 4.2 also minimises the power loss $\sigma|\mathbf{E}|^2$.

The next phase is to discretise the problem and select the presentation for the test function v. For simplicity, let us consider only a two-dimensional case. The usual choice for elliptic problems is to use the same presentation for both v and the unknown ϕ. This is called *Galerkin's* method and one advantage of this choice is that the resulting system is symmetric and in our case also positive definite since $\sigma > 0$. Let us now restrict to the so-called nodal FEM where the v and ϕ are presented as scalar functions which are defined with the aid of *basis functions* that depend on nodal values. In traditional FEM the discretization of the domain has to be *conformal*, which in the case of triangular mesh requires that neighbouring triangles share exactly one edge and two vertices (nodes). The most simple, first order polynomial basis function can now be defined to the compact area around each node restricted by the neighbouring elements. The concept of conformal mesh and nodal basis function is clarified in Figure 4.4 where a simple example of a triangulation of a square is shown. In the middle of the figure a single linear basis function is also presented.

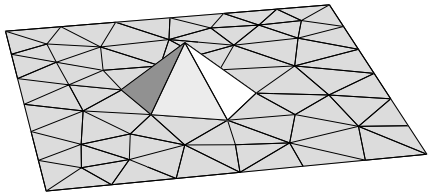

Figure 4.4: Example of a conformal triangular FEM mesh. In the centre of the mesh a single basis function is exemplified.

One can see that the domains of the basis functions associated with neighbouring nodes have an overlap.

If we now write the test function v and unknown scalar potential ϕ as a sum of the basis functions, the discretized problem can be written as

$$\int_V \sum_{i=1}^{N} \sum_{j=1}^{N} \nabla u_i \cdot \sigma \nabla u_j \, dV = -j\omega \int_V \sum_{i=1}^{N} \nabla u_i \cdot \sigma \mathbf{A}_0 \, dV, \tag{4.3}$$

where N is the number of nodes. This discrete system can be written as a linear equation $\mathbf{Ax} = \mathbf{b}$ where the values of $\mathbf{A}$ and $\mathbf{b}$ are determined by Equation 4.3. As the domain of each basis function is finite, the matrix $\mathbf{A}$ is sparse. As the direct solution of sparse matrix equations is feasible only with relatively small systems, one usually solves the resulting equation iteratively.

In publication **II** a non-conformal mesh was used because of the complexity of mesh generation. Non-conformal meshes require a procedure that ensures that the basis functions form a continuous presentation for test and unknown functions. In publication **II** the so-called *hanging nodes* were forced to values that ensure the continuity by adding the linear dependencies of the node values to the resulting matrix equation. Other possibilities

include, for example, the use of Lagrangian multipliers. See e.g. [50] for summary of different approaches for bioelectromagnetic FEM simulations. A somewhat similar scheme for finite-integration technique is presented in [51].

Because the physical quantity we are interested in is the induced electric field as presented in Equation 2.14, we have to compute the gradient of the scalar potential solution. In the finite-difference methods, this numerical derivation can be complicated due to the boundaries of different materials, i.e. discontinuities of the conductivity, see e.g. [52] for an example. In the FEM, the gradient can be computed simply from the gradients of the basis functions.

4.4 Modelling of Sources

Correct modelling of the source of the exposure is essential for dosimetric simulations. In practice, the requirement can be very difficult as the detailed electrical operation of the exposing device is often needed for accurate modelling. In some cases, for example in the case of a tram, the electromagnetic fields are a side effect, not an integral part of the device. In those cases even the manufacturer may not have detailed information about the fields generated by the device under study. Often the manufacturer is also not willing to reveal the full details of operation as it is considered a trade secret. In these cases the construction of the source for exposure simulation is a complicated work. It should be noted, though, that there are several technical specifications for all electrically powered equipment, including trams, that affect also the level of electromagnetic fields that such devices generate.

An important principle that can be utilised in the simulations is the concept of *equivalent source*. For the determination of exposure one does not need to model the whole device under study. It is sufficient to generate equivalent field distribution and interaction on the region of the human body. This task is rather easy for quasi-static magnetic fields, but not so easy, for example, in the case of a mobile phone or other RF sources located in close vicinity to the body. This is due to the complicated electromagnetic interaction between the device and body which affects, among other things, the antenna feed impedance and radiation properties. Modelling of quasi-static magnetic fields is easier, as the body is not ferromagnetic and as such does not alter the distribution of the source magnetic flux density, i.e. the coupling between the source and body is minuscule.

4.4.1 Low-Frequency Quasi-Static Sources

The strong magnetic field usually originates from strong currents, hence in practice strong sources of magnetic field exposure are due to devices which use considerable current from the electricity grid, such as welding machines, large electric furnaces, power lines of trams, etc. Another source of even stronger fields results from the very strong magnets found in magnetic resonance imaging scanners. Examples of extremely low-frequency exposure computations for different types of sources can be found *inter alia* in [52–54].

If the exposure simulation is done using the scalar potential formulation, one has to determine the source vector potential $\mathbf{A}_0$ for Equation 2.13. If the current distribution of the source is known, one can determine the $\mathbf{A}_0(\mathbf{r})$ as [5]

$$\mathbf{A}_0(\mathbf{r}) = \frac{\mu_0}{4\pi} \int_V \frac{\mathbf{J}(\mathbf{r}')}{|\mathbf{r} - \mathbf{r}'|} \, d\mathbf{r}' \tag{4.4}$$

where the integration volume V is the domain of the source current (outside of the body, as we do not consider the contact currents). Therefore, if the source current distribution is known, the determination of the source vector potential is straightforward. Unfortunately, the current distribution is easy to determine only in certain simple cases such as power lines. In more complicated cases, the equivalent source may be constructed by simulating the source structure or by using measurement. As the measurement of non-unique vector potential is not possible, the source magnetic flux has to be measured in a volume of the body.

In order to use the measured source data, we need some method do derive one possible vector potential whose curl is equivalent to the measured data (within the limits of measurement accuracy). One approach is to use a group of magnetic dipoles or a multipole expansion and fit the moments to the measurements [55–58]. This approach is also used in paper **II**, where a group of magnetic dipoles were used to model the battery currents of a mobile phone. When the *magnetic dipole moment* $\mathbf{m}$ is known, the magnetic flux density induced by the magnetic dipole can be written as [5]

$$\mathbf{B}(\mathbf{r}) = \frac{\mu_0}{4\pi}\left(\frac{3\hat{\mathbf{r}}(\hat{\mathbf{r}}\cdot\mathbf{m})-\mathbf{m}}{|\mathbf{r}|^3}\right), \tag{4.5}$$

where $\hat{\mathbf{r}}$ denotes a unit vector in the direction of $\mathbf{r}$. The construction of the source vector potential is very simple, as the corresponding $\mathbf{A}_0$ can be written as

$$\mathbf{A}_0(\mathbf{r}) = \frac{\mu_0}{4\pi}\frac{\mathbf{m}\times\mathbf{r}}{|\mathbf{r}|^3}. \tag{4.6}$$

This vector potential fulfils the Coulomb's gauge $\nabla\cdot\mathbf{A}_0 = 0$.

One can also approximate the current distribution $\mathbf{J}$ with some appropriate parameterised current and fit the parameters of the source to the measured field. The $\mathbf{A}_0$ can then be computed using the fitted current distribution from Equation 4.4. This approach is used in paper **I**. The main difficulty of this approach is the choice of the current distribution and the parametrisation so that the field distribution is correctly reproduced.

4.4.2 High Frequency Sources

At higher frequencies, a typical source of exposure is an antenna. The type of antenna depends on the equipment under study; the antenna of a radar, for instance, is very different from an antenna of a personal communication device. The coupling of the RF field into the body is naturally also different in these cases. The RF exposure scenarios can be classified as near- or far-field scenarios depending on the coupling between the antenna and the body. In the case of far-field exposure, the modelling of the source is much easier as the coupling between the antenna and the body can be omitted and the source can be modelled by using, for example, simple plane-wave expansion, or by using a more general presentation and Hyugen's principle. Unfortunately, considering the far-field exposure is often not sufficient, as from the dosimetric point of view the most challenging case is the inhomogeneous near field exposure. In such cases, the proximity of the human body can affect the input impedance of the antenna elements [49]. Because of this, the approach similar to that used for equivalent low-frequency source is not feasible and one has to simulate the operation of the antenna in more detail.

In this thesis, the only high-frequency source is the small indoor base station antenna studied in publication **V**. In that case the geometrical information of the antenna was not available and the technical information sheet available from the manufacturer was insufficient for detailed dosimetric simulations. The antenna had two different radiating elements, one for lower a frequency band and other for wide a higher frequency band. The operation of the feed network of these elements was also unclear. However, in our case the change of the feed impedance does not have as strong effect on the radiation properties as in the case of an antenna group. The change in impedance affects the matching of the antenna and the feed.

The equivalent model of the antenna in publication **V** was constructed using photographs of the opened antenna and measurements of the physical dimensions by a slide gauge. The original coaxial feed of the higher frequency band element was replaced with a voltage gap located close to the estimated position of the maximum field intensity. As only the higher frequency band was considered, the whole lower band element was simulated as a passive metallic structure. In the FDTD simulation, the losses were not considered and the whole structure was assumed to be perfectly conducting. The losses of the whole antenna structure, including the feed network and cables, were taken into account by a single loss factor that connects the input and radiation power of the antenna. This factor was determined from the antenna efficiency measurements. As seen in publication **V**, the used approach gave very good results when compared to the measurements.

5 Summary of Publications

I *Numerical assessment of induced ELF currents in human head due to the battery current of a digital mobile phone*

The distribution of the pulsed magnetic field in the proximity of a GSM phone is measured and a planar equivalent source of the battery current is constructed for numerical simulation. The induced current inside the human cranium is computed using two different numerical methods, FEM and FIT, and the results are compared to each other and to the guidelines of ICNIRP. The induced currents were found to be significantly lower than the restriction limits.

II *Magnetic-field-induced ELF currents in a human body by the use of a GSM phone*

A new equivalent model is constructed for the battery current problem due to the shortcomings of the equivalent model in **I**. Additionally, a new solver capable of computing solution to locally refined models is implemented. These developments enable the solving of additional exposure scenarios with a considerably more detailed model. A test for the orientation and position of the mobile phone is also included and it is seen that the results are very distance sensitive. Nevertheless, the currents are well below the restriction limits.

III *Performance of convolutional PML absorbing boundary conditions in finite-difference time-domain SAR calculations*

The validity and performance of a convolutional PML absorbing boundary is studied and the results are compared to recently published contradictory results found in the literature. The performance of the CPML is compared to that of the regular PML. It is demonstrated that with correctly selected parameters the CPML performs better than the traditional PML in certain types of SAR computations and the air layer between the PML boundary condition and the object can be made very small.

IV *The effect of finite-difference time-domain resolution and power-loss computation method on SAR values in plane-wave exposure of Zubal phantom*

The effect of model resolution is studied using two different versions of Zubal phantom. A finer resolution model is constructed from the coarse one by dividing each material voxel into eight new voxels with similar tissue in order to keep the geometry of the models comparable. Also the different interpolation choices used in the computation of the SAR values for each voxel are studied. Results show that varying the resolution, averaging method and power loss computation method can cause variation of tens of percents in the SAR values.

V *Numerical specific absorption rate analysis and measurement of a small indoor base station antenna*

A computational model of a simple indoor base station antenna is constructed. The near field of the antenna is measured in free space and with a liquid flat phantom. Also the efficiency of the antenna is measured for calibration of output power levels between the measurements and simulation. The measurements and simulations are compared to validate the numerical model. This validated model is then used to determine the SAR values due to the exposure in very close proximity to the antenna. The obtained results are compared to the limits and guidelines in order to estimate the compliance of the antenna. For this antenna configuration the equivalent power density gives conservative compliance distances.

VI *Computational estimation of magnetically induced electric fields in a rotating head*

In this theoretical study four different head models are used to study the motion-induced fields due to rotational head movements in a static homogeneous magnetic field. The results are in good agreement with recently published measurements found in the literature. In addition, coarse estimates for field intensities near the retina and inner ears are computed. The obtained result is compared to current estimates on the threshold values for phosphenes. The results show that the 1 T s^{-1} change in magnetic flux density can induce an electric field of 50 mV m^{-1} near retinas and 100 mV m^{-1} near vestibular organs.

References

[1] M. Piccolino, "Animal electricity and the birth of electrophysiology: The legacy of Luigi Galvani," *Brain Research Bulletin*, vol. 46, no. 5, pp. 381–407, Jul 1998.

[2] C. L. Sulzberger, "Triumph of AC. 2. The battle of the currents," *IEEE Power and Energy Magazine*, vol. 1, no. 4, pp. 70–73, Jul–Aug 2003.

[3] H. Nyberg and K. Jokela, Eds., *Sähkömagneettiset kentät*. Säteilyturvakeskus, 2006.

[4] S. Crozier and F. Liu, "Numerical evaluation of the fields induced by body motion in or near high-field MRI scanners," *Progress in Biophysics and Molecular Biology*, vol. 87, pp. 267 – 278, 2005.

[5] J. D. Jackson, *Classical Electrodynamics*, 3rd ed. John Wiley & Sons, Inc., 1999.

[6] T. W. Dawson, J. D. Moerloose, and M. A. Stuchly, "Comparison of magnetically induced ELF fields in humans computed by FDTD and scalar potential FD codes," *Applied Computational Electromagnetic Society Journal*, vol. 11, no. 3, pp. 63–71, 1996.

[7] P. J. Dimbylow, "Induced current densities from low-frequency magnetic fields in a 2 mm resolution, anatomically realistic model of the body," *Physics in Medicine and Biology*, vol. 43, no. 2, pp. 221–230, 1998.

[8] F. Liu and S. Crozier, "Electromagnetic fields inside a lossy, multilayered spherical head phantom excited by MRI coils: models and methods," *Physics in Medicine and Biology*, vol. 49, pp. 1835 – 1851, 2003.

[9] O. P. Gandhi, J. F. Deford, and H. Kanai, "Impedence method for calculation of power deposition patterns in magnetically induced hyperthermia," *IEEE Transactions on Biomedical Engineering*, no. 10, pp. 644–651, Oct 1984.

[10] A. Barchanski, M. Clemens, H. D. Gersem, and T. Weiland, "Efficient calculation of current densities in the human body induced by arbitrarily shaped, low-frequency magnetic field source," *Journal of Computational Physics*, vol. 214, pp. 81–95, May 2006.

[11] A. Barchanski, M. Clemens, E. Gjonaj, H. De Gersem, and T. Weiland, "Large-scale calculation of low-frequency-induced currents in high-resolution human body models," *IEEE Transactions on Magnetics*, vol. 43, no. 4, pp. 1693–1696, Apr 2007.

[12] K. R. Foster and H. P. Schwan, "Dielectric properties of tissues and biological materials: a critical review," *Critical Reviews in Biomedical Engineering*, vol. 17, no. 1, pp. 25–104, 1989.

[13] J. P. Reilly, *Applied Biolectricity: From Electrical Stimulation to Electropathology*. New York: Springer-Verlag, 1998.

[14] C. Gabriel, S. Gabriel, and E. Corthout, "The dielectric properties of biological tissues: I. Literature survey," *Physics in Medicine and Biology*, vol. 41, pp. 2231–2249, 1996.

[15] S. Gabriel, R. Lau, and C. Gabriel, "The dielectric properties of biological tissues: II. Measurement in the frequency range 10 Hz to 20 GHz," *Physics in Medicine and Biology*, vol. 41, pp. 2251–2269, 1996.

[16] S. Gabriel, R. Lau, and C. Gabriel, "The dielectric properties of biological tissues: III. Parametric models for the dielectric spectrum of tissues," *Physics in Medicine and Biology*, vol. 41, pp. 2271–2293, 1996.

[17] A. Barchanski, H. D. Gersem, E. Gjonaj, and T. Weiland, "Impact of the displacement current on low-frequency electromagnetic fields computed using high-resolution anatomy models," *Physics in Medicine and Biology*, vol. 50, no. 19, pp. N243–N249, Oct 2005.

[18] International Commission of Non-Ionizing Radiation Protection, "Guidelines for limiting exposure to time-varying electric, magnetic, and electromagnetic fields (up to 300 GHz)," *Health Physics*, vol. 74, no. 4, pp. 494–522, Apr 1998.

[19] P. M. Glover and R. Bowtell, "Measurement of electric fields induced in a human subject due to natural movements in static magnetic fields or exposure to alternating magnetic field gradients," *Physics in Medicine and Biology*, vol. 53, no. 2, pp. 361–373, 2008.

[20] R. L. Carpenter, "Ocular effects of microwave radiation," *Bulletin of the New York Academy of Medicine*, vol. 55, no. 11, pp. 1048–1057, Dec 1979.

[21] P. Glover, I. Cavin, W. Qian, R. Bowtell, and P. Gowland, "Magnetic-field-induced vertigo: A theoretical and experimental investigation," *Bioelectromagnetics*, vol. 28, no. 5, pp. 349 – 361, 2007.

[22] J. C. Lin, "Hearing microwaves: the microwave auditory phenomenon," *IEEE Antennas and Propagation Magazine*, vol. 43, no. 6, pp. 166–168, Dec 2001.

[23] World Health Organization, "Extremely low frequency fields environmental health criteria monograph no.238," 2007.

[24] A. W. Wood, "Extremely low frequency (ELF) electric and magnetic field exposure limits: Rationale for basic restrictions used in the development of an Australian standard," *Bioelectromagnetics*, vol. 29, no. 6, pp. 414 – 428, 2008.

[25] *IEEE Std C95.6-2002 IEEE standard for safety levels with respect to human exposure to electromagnetic fields, 0-3 kHz*, IEEE Std. C95.6-2002, 2002.

[26] *IEEE Std C95.1-2005 IEEE Standard for Safety Levels with Respect to Human Exposure to Radio Frequency Electromagnetic Fields, 3 kHz to 300 GHz*, IEEE Std., 2006.

[27] International Commission on Non-Ionizing Radiation Protection, "Guidance on determining compliance of exposure to pulsed and complex non-sinusoidal waveforms below 100 kHz with ICNIRP guidelines," *Health Physics*, vol. 84, no. 3, pp. 383–387, Mar 2003.

[28] International Commission of Non-Ionizing Radiation Protection, "Guidelines on limits of exposure to static magnetic fields," *Health Physics*, vol. 96, no. 4, pp. 504–514, Apr 2009.

[29] J. P. Reilly and A. M. Diamant, "Spatial relationships in electrostimulation: application to electromagnetic field standards," *IEEE Transactions on Biomedical Engineering*, vol. 50, no. 6, pp. 783–785, Jun 2003.

[30] P. Dimbylow, "Quandaries in the application of the ICNIRP low frequency basic restriction on current density," *Physics in Medicine and Biology*, vol. 53, no. 1, pp. 133–145, Jan 2008.

[31] *IEEE Std C95.3-2002 (R2008) IEEE recommended practice for measurements and computations of radio frequency electromagnetic fields with respect to human exposure to such fields, 100 kHz-300 GHz*, IEEE Std., 2002.

[32] A. R. Shapiro, R. F. Lutomirski, and H. T. Yura, "Induced fields and heating within a cranial structure irradiated by an electromagnetic plane wave," *IEEE Transactions on Microwave Theory and Techniques*, vol. 19, no. 2, pp. 187–196, Feb 1971.

[33] H. Massoudi, C. H. Durney, and C. C. Johnson, "Long-wavelength analysis of plane wave irradiation of an ellipsoidal model of man," *IEEE Transactions on Microwave Theory and Techniques*, vol. 25, no. 1, pp. 41–46, Jan 1977.

[34] C. H. Durney, "Electromagnetic dosimetry for models of humans and animals: A review of theoretical and numerical techniques," *Proceedings of the IEEE*, vol. 68, no. 1, pp. 33–40, Jan 1980.

[35] S. Caorsi, M. Pastorino, and M. Raffetto, "Analytic sar computation in a multilayer elliptic cylinder for bioelectromagnetic applications," *Bioelectromagnetics*, vol. 20, no. 6, pp. 365–371, Sep 1999.

[36] P. Ljung, C. Winskog, A. Persson, C. Lundstrom, and A. Ynnerman, "Full body virtual autopsies using a state-of-the-art volume rendering pipeline," *IEEE Transactions on Visualization and Computer Graphics*, vol. 12, no. 5, pp. 869–876, Sept–Oct 2006.

[37] A. W. Liew and H. Yan, "Current methods in the automatic tissue segmentation of 3D magnetic resonance brain images," *Current Medical Imaging Reviews*, vol. 2, no. 1, pp. 91–103, Feb 2006.

[38] M. J. Ackerman, "The visible human project," *Proceedings of the IEEE*, vol. 86, no. 3, pp. 504–511, Mar 1998.

[39] M. S. Chung, "Visible korean human. improved serially sectioned images of the entire body," in *Proc. 27th Annual International Conference of the Engineering in Medicine and Biology Society IEEE-EMBS 2005*, 2005, pp. 6563–6566.

[40] A. Christ, W. Kainz, E. Hahn, K. Honegger, M. Zefferer, E. Neufeld, W. Rascher, R. Janka, W. Bautz, J. Chen, B. Kiefer, P. Schmitt, H. P. Hollenbach, J. X. Shen, M. Oberle, A. Kam, and N. Kuster, "The Virtual Family - Development of anatomical CAD models of two adults and two children for dosimetric simulations," 2008, manuscript in preparation.

[41] T. W. Dawson, K. Caputa, and M. A. Stuchly, "High-resolution organ dosimetry for human exposure to low-frequency electric fields," *IEEE Transactions on Power Delivery*, vol. 13, no. 2, pp. 366–373, Apr 1998.

[42] T. Nagaoka and S. Watanabe, "Postured voxel-based human models for elecromagnetic dosimetry," *Physics in Medicine and Biology*, vol. 53, pp. 7047–7061, 2008.

[43] K. S. Yee, "Numerical solution of initial boundary value problems involving Maxwell's equations in isotropic media," *IEEE Transactions on Antennas and Propagation*, vol. 14, pp. 302–307, 1966.

[44] A. Taflove and M. E. Brodwin, "Computation of the electromagnetic fields and induced temperatures within a model of the microwave-irradiated human eye," *IEEE Transactions on Microwave Theory and Techniques*, vol. 23, no. 11, pp. 888–896, Nov 1975.

[45] A. Taflove and S. C. Hagness, *Computational Electrodynamics: The Finite-Difference Time-Domain Method*, 3rd ed. Artech House, 2005.

[46] R. P. Findlay and P. J. Dimbylow, "Variations in calculated SAR with distance to the perfectly matched layer boundary for a human voxel model," *Physics in Medicine and Biology*, vol. 51, pp. N411–N415, 2006.

[47] J. Jin, *The Finite Element Method in Electromagnetics*, 2nd ed. John Wiley & Sons, Inc., 2002.

[48] F. J. C. Meyer, D. B. Davidson, U. Jakobus, and M. A. Stuchly, "Human exposure assessment in the near field of GSM base-station antennas using a hybrid finite element/method of moments technique." *IEEE Transactions on Biomedical Engineering*, vol. 50, no. 2, pp. 224–233, Feb 2003.

[49] M. J. van Wyk, M. Bingle, and F. J. C. Meyer, "Antenna modeling considerations for accurate SAR calculations in human phantoms in close proximity to GSM cellular base station antennas." *Bioelectromagnetics*, vol. 26, no. 6, pp. 502–509, Sep 2005.

[50] P. Schimpf, D. Haynor, and Y. Kim, "Object-free adaptive meshing in highly heterogneous 3-D domains," *International Journal of Bio-Medical Computing*, vol. 40, pp. 209–225, 1996.

[51] A. Barchanski, T. Steiner, H. De Gersem, M. Clemens, and T. Weiland, "Local grid refinement for low-frequency current computations in 3-D human anatomy models," *IEEE Transactions on Magnetics*, vol. 42, no. 4, pp. 1371–1374, April 2006.

[52] F. Liu, H. Zhao, and S. Crozier, "On the induced electric field gradients in the human body for magnetic stimulation by gradient coils in MRI," *IEEE Transactions on Biomedical Engineering*, vol. 50, no. 7, pp. 804–815, 2003.

[53] O. P. Gandhi, G. Kang, D. Wu, and G. Lazzi, "Currents induced in anatomic models of the human for uniform and nonuniform power frequency magnetic fields," *Bioelectromagnetics*, vol. 22, no. 2, pp. 112–121, 2001.

[54] J. Cheng, M. A. Stuchly, C. DeWagter, and L. Martens, "Magnetic field induced currents in a human head from use of portable appliances," *Physics in Medicine and Biology*, vol. 40, no. 4, pp. 495–510, Apr 1995.

[55] R. G. Olsen and C. E. Lyon, "Modeling of extremely low frequency magetic field sources using multipole techniques," *IEEE Transactions on Power Delivery*, vol. 11, pp. 1563–1570, 1996.

[56] L. E. Zaffanella, T. P. Sullivan, and I. Visintainer, "Magnetic field characterization of electrical appliances as point sourced through in situ measurements," *IEEE Transactions on Power Delivery*, vol. 12, no. 1, pp. 443–450, Jan 1997.

[57] K. Yamazaki and T. Kawamoto, "Simple estimation of equivalent magnetic dipole moment to characterize elf magnetic fields generated by electric appliances incorporating harmonics," *IEEE Transactions on Electromagnetic Compatibility*, vol. 43, no. 2, pp. 240–245, May 2001.

[58] S. Nishizawa, H.-O. Ruoß, F. M. Landstorfer, and O. Hashimoto, "Numerical study on an equivalent source model for inhomogeneous magnetic field dosimetry in the low-frequency range," *IEEE Transactions on Biomedical Engineering*, vol. 51, no. 4, pp. 612–616, Apr 2004.